A Low-cost and Portable System for Real-time Impedimetric Measurements and Impedance Spectroscopy of Sensors

Michele Rossi, Marco Bennati, Federico Thei, and Marco Tartagni

ARCES – Advanced Research Center on Electronic Systems

Second School of Engineering, University of Bologna - Via Venezia 52, 47521 – Cesena (FC), Italy

mrossi@arces.unibo.it, mbennati@arces.unibo.it, fthei@arces.unibo.it, mtartagni@arces.unibo.it

Abstract— **This paper presents a low cost and portable system that is able to perform real time or spectra impedance characterization of impedimetric sensors interfaces. It is also able to perform simple amperometric measurements for real-time DC current-voltage characterization or studies of the behavior of the sensor with respect to different target stimuli. Due to its flexible design, the system can be easily adapted to different applications and experimental requirements. Synthetic devices under test (DUTs) were used for testing purposes and the performances have been compared to those obtained using a commercial dedicated impedance analyzer. The system allows displaying results in Nyquist and Bode plots using a friendly graphical user interface. Results show remarkable fair accuracy, considering the much lower price, smaller sizes and flexibility of use of the developed system.**

Keywords – Biosensors; Sensor interfaces; Impedance spectroscopy; Real time; Amperometry measurements.

I. INTRODUCTION

In the last decade, the convergence of nanotechnology with biology and medicine and the ability to fabricate structures using standard wafer-scale semiconductor processing techniques has shown an emerging and evolving interest in the development of new classes of rapid, sensitive, and reliable biosensors devices, such as nanowires and carbon nanotubes [1][2][3][4][5].

These devices could have a great impact on many application fields related to our life: from health-care and environment, to food production and bio-warfare thanks to their properties of electrical, label-free and real time readout. Moreover, the possibility of integration of this class of sensors with the readout structure makes them even more interesting. However, the integration of sensors with interfaces demands a quick although accurate knowledge of electrical parameters (such as impedance, noise and bandwidth) [6] and their related behaviors to target stimulus, in order to understand the design constraints of the readout systems. Another important issue to point out is the lack of instrumentation able to perform both impedance spectroscopy and real-time impedance measurements in order to identify the electrical parameters model and real time behaviors of biosensors depending upon the specific structure and fabrication process [7][8].

For the above reasons, there is a demand for low cost, portable readout structures able to perform accurate preliminary tests on biosensors and/or to perform routine tests with respect to experimental conditions avoiding skilled personnel and bulky instruments.

The main characteristics needed for the readout system are:

- Compact and low cost;
- Flexible to cope with different kind of biosensors;
- Able to perform parallel acquisitions, allowing high throughput;
- Perform differential measurements in order to further increase sensitivity and selectivity;
- Perform a full characterization of impedance in the magnitude and in the phase, since the latter could offer a better understanding of the surface molecular interaction [9].

This paper presents a low cost, versatile and portable test board for sensors implementing a two electrode potentiostat, conjugated with a lock-in technique for complex impedance detection which allows obtaining comprehensive information on the impedance magnitude and phase (Figure 1). More specifically, the instrument has been designed to be interfaced to bionanosensors, such as nanowires or carbon nanotubes; however it is not the purpose of this paper to describe a single specific application related to this kind of biosensors, but rather investigate the potentiality of this system interface to be used for different kinds of sensors.

Section II will show the system architecture and functionalities. Section III will present the developed acquisition board features and working principles. Section IV will show the LabVIEW software interface and the implemented digital signal conditioning process. Finally, Section V will present the results of tests performed on synthetic DUTs simulating sensors behaviors and a comparison between the developed system and a commercial impedance analyzer.
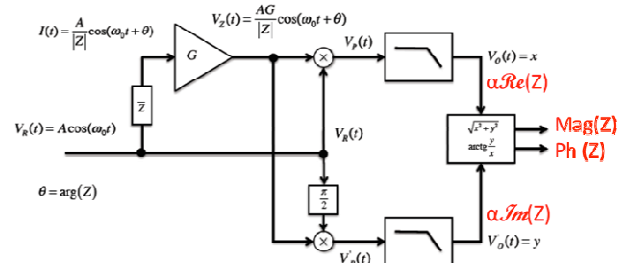
Figure 1. Schematic of the lock-in technique for complex impedance detection.

II. SYSTEM STRUCTURE AND SETUP

The system consists of a custom printed circuit mother board (PCB) hosting both the DUT and the readout interface. The latter performs the readout of the current signal coming out of the sensors in response to a sinusoidal or DC V_{ref} signal generated by a waveform generator (Tektronix AFG 3102 [10]) and digitized by a National Instruments 6009 DAQ card [11] whose output is sent to a laptop for storing and online (or post) processing using a LabView interface.

The above approach, based on performing the filtering and data manipulations in the digital domain, allows the system to be particularly flexible, maintaining a simple analog front-end for different applications with respect to the system required performances.

In particular, the developed system is designed to be as much versatile as possible allowing to perform the following measurements in lock-in readout configuration:

1) Real-time DC current measurements;
2) DC voltage sweeps, for device characterization;
3) Real-time AC measurements of sensor impedance/admittance magnitude and phase;
4) Impedance AC spectra.

The graphical user interface is able to reconstruct in real time both Nyquist and Bode plots.

III. ACQUISITION BOARD INTERFACE

The designed acquisition board (block diagram shown in Figure 2) is characterized by the following features:

- Two identical and independent readout branches to allow differential measurements on sensors (Z_{ref} and Z_{sens} in Figure 2). The board could be used for array of sensors as well;
- Addressable switching system to select, independently on the two branches, single sensors in a chip array (see Figure 1);
- Operating frequency in the range of 0.1Hz-2KHz (typical for nanowires or nanotube sensors lock-in readout measurements) [2][4][5][8][12][13];
- DC measurements bypassing the demodulation stage (this possibility is represented with switches on each branch of Figure 2);
- Four different current ranges selectable by mechanical switch, in particular ±7.85µA, ±785nA, ±78.5nA, ±7.85 nA.
- Auxiliary potential (V_{bulk}) control circuit to set the back-gate and/or liquid gate potential of nanowires or nanotubes chip [2][13][15].
- Real time parallel measurements of both real and imaginary part of sensors impedance using two independent demodulators for each branch of the system.
- Custom designed socket (4x4 cm) for hosting the DUT/sensor.

Special attention was paid to the four layer PCB layout in order to shield as much as possible the analog signals on the board from external noise sources.
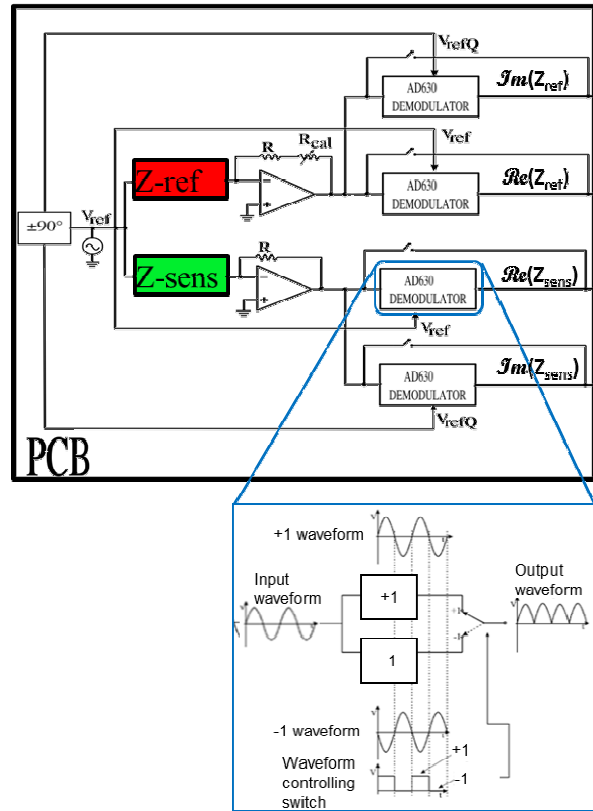
Figure 2. Block diagram of the designed acquisition board. The zoom shows the working principle of the AD 630 demodulator. The switch is driven by a comparator that compares the reference signal (V_{ref} and V_{refQ}) with its DC offset level, resulting in a square wave in-phase with the reference signal.

Each branch of the circuit can be represented by two stages: a transimpedance input amplifier that converts the current signal coming from sensors to an amplified voltage signal prior to be sent to the integrated circuit (AD630) that performs the phase-sensitive detection. The signal is preamplified by an AD822 due to its low-power rail-to-rail and low noise operating performances (13 nV/√Hz @ 10 kHz) and low input bias current [16].

The demodulation is implemented by using an AD630 since it is currently used in precision signal processing and instrumentation applications requiring wide dynamic range [16].

The AD630 demodulator is configured to have a gain of ±1 and, since the positive or negative gain is controlled by a switch controlled by a comparator (zoom in Figure 2), thus the demodulator multiplies the input waveform for a unitary square wave whose Fourier series is [17]:

$$V_{square}(t) = \frac{4}{\pi} \cdot \sum_{k=1}^{\infty} \left(\frac{\sin((2k-1) \cdot \omega t)}{2k-1} \right) \quad (1)$$

and the reference waveform sent to both the DUT and the comparator input is:

$$V_{ref} = V_i \cdot \sin(\omega_i t) \quad (2)$$

the output of the in-phase branches of the circuit is:

$$V_o(t) = -V_i \cdot \left(\frac{R_f}{Z_{sens}} \right) \cdot \sin(\omega_i t + \varphi) \cdot \left(\frac{4}{\pi} \right) \cdot \sum_{k=1}^{\infty} \left(\frac{\sin((2k-1) \cdot \omega t)}{2k-1} \right) \quad (3)$$

where R_f and Z_{sens} are respectively the selected feedback resistance, which sets the range of measurements of the system, and the sensor impedance. As can be seen, the output signal presents a high harmonic content associated to the square wave components of the signal.

The output of the two "real part" branches of the PCB that are externally digitized and filtered could be derived from (3) as:

$$V_o(t) = -V_i \cdot \left(\frac{R_f}{Z_{sens}} \right) \cdot \left(\frac{2}{\pi} \right) \cdot \cos(\varphi) = \alpha \cdot \mathrm{Re}(Y_{sens}) \quad (4)$$

Similarly, the output of the quadrature branches, in which the comparator input is shifted of 90° (V_{refQ} in Figure 2), of the circuit is:

$$V_o(t) = -V_i \cdot \left(\frac{R_f}{Z_{sens}} \right) \cdot \sin(\omega_i t + \varphi) \cdot \left(\frac{4}{\pi} \right) \cdot \sum_{k=1}^{\infty} \left(\frac{\cos((2k-1) \cdot \omega t)}{2k-1} \right) \quad (5)$$

by which it is possible to obtain the output of the two "imaginary part" branches of the PCB, then externally digitized and filtered yielding:

$$V_o(t) = -V_i \cdot \left(\frac{R_f}{Z_{sens}} \right) \cdot \left(\frac{2}{\pi} \right) \cdot \sin(\varphi) = \alpha \cdot \mathrm{Im}(Y_{sens}) \quad (6)$$

Figure 3 shows a picture of the PCB where on one side are arranged:

- An input signal SMB connector for the Vref,
- A dual power supply connector,
- 4 output SMB connectors (Re$_1$, Im$_1$ Re$_2$ Im$_2$).

The socket connectors provides the power supply, Ground, V_{ref} and V_{bulk} signals to the PCB plug interfaces for different (eventually based on active components) solutions and connects the selected sensor to the selected branch of the circuit (see Figure 1).
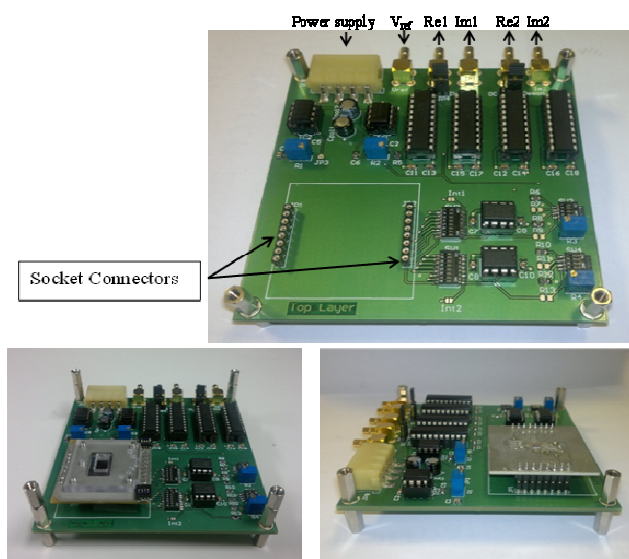
Figure 3.   Picture of designed acquisition board PCB interface.

IV.   LABVIEW INTERFACE AND FILTER DESIGN

The implemented software interface allows to:

- control the function generator and set V_{ref} waveform properties (frequency, amplitude, DC offset) using the USB interface;
- control the NI-DAQ, setting the proper (adapted to the V_{ref} frequency) sampling rate and DAQ acquisition voltage range;
- simultaneously control the real time signal value for the four outputs of the acquisition board to finally have the mean Re$_1$, Im$_1$ Re$_2$ Im$_2$ values;
- perform real time calculation to finally display the real time Nyquist diagram of the admittance (or impedance), as well as Phase and Magnitude values and calculate the simple RC equivalent circuit.
- save data in users-specified text files.

The main signal conditioning process (represented in Figure 4) was segmented into 3 stages: two stages implementing finite impulse response digital low-pass filters (FIR Kaiser window) and one devoted to decimation. Weight taps have been calculated with MATLAB to have the best configuration for all the frequency in the functioning range. In order to optimize the computational resources, an adaptive filtering based on the input frequency (f_i) and the signal band (user selectable) cut off frequency (f_{cfinal}) was implemented in the software interface.

The interface also allows selecting the highest harmonic of the signal (see (3) and (5)) to be considered following the Nyquist criterion, consequently changing the sampling ratio of the NI DAQ.
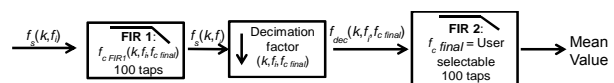
Figure 4.   Representation of the adaptive two stages low pass FIR filter implemented in the LabView interface .

In order to perform real time, 4-channel measurements with a low final cutoff frequency (usually 1 or 0.1 Hz) and relatively limited computational resources (e.g., if using a laptop), a good trade-off between performances and computational complexity has been found to be the cascade of two 100-tap adaptive filters.

The two stages are dimensioned to satisfy the condition of same ratio between cutoff frequency and bandwidth:

$$\frac{f_{cFIR1}}{f_s} = \frac{f_{cfinal}}{f_{dec}}, \quad (7)$$

whose expression, considering $f_{dec} = 2 \cdot f_{c\ FIR1}$, allows calculating the first filter cutoff frequency (f_{cFIR1}) and the decimation ratio as:

$$f_{cFIR1} = \sqrt{\frac{f_{cfinal} \cdot f_s}{2}} \quad (8)$$

$$dec\ ratio = \frac{f_s}{f_{dec}} = \sqrt{\frac{f_s}{2 \cdot f_{cfinal}}} \quad (9)$$

The obtained filtered voltage signals are then real time manipulated to evaluate magnitude and phase from each branch of the circuit:

$$\left|V_o(t)\right| = \sqrt{\text{Re}^2\{V_o(t)\} + \text{Im}^2\{V_o(t)\}} = V_i \cdot \left(\frac{R_f}{|Z_{sens}|}\right) \cdot \left(\frac{2}{\pi}\right) \quad (10)$$

$$\varphi = \tan^{-1}\frac{\text{Im}\{V_o(t)\}}{\text{Re}\{V_o(t)\}} \quad (11)$$

Other data manipulation implemented in the LabView software interface also allows to calculate in real-time the equivalent resistance and capacitance of the series and parallel RC models.

Figure 5 shows the implemented LabView interface.
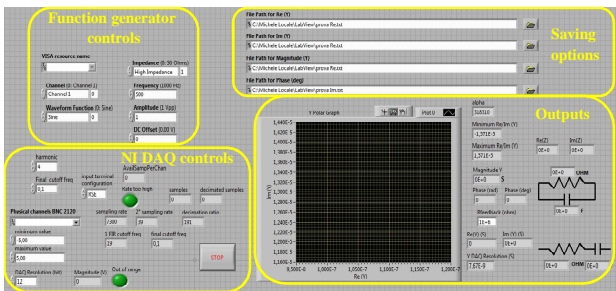
Figure 5.   Implemented LabView interface.

V.   RESULTS

Preliminary AC real time tests on synthetic DUTs (resistors, capacitors and RC combinations) in different measurement ranges and at different frequencies were performed connecting the DUT between V_{ref} and a selected socket connector. In particular, Vishay precision resistor of 1MΩ and 10MΩ, 0.005% tolerance and Dale RNX-3/8 100MΩ resistor, 1% tolerance and capacitor of 100pF and 1nF were used.

Figure 6 shows results of performed measurements using an R=1MΩ, C=1nF parallel circuit. The figure shows a full scale view of the admittance in the Nyquist plane, while the zoomed version shows the details of the measurement. As can be seen in the figure zoom, a small phase shift caused by parasitic effects is present; this could be compensated in post processing after the calibration.

Table I sums up the different configurations for the four different selectable ranges of measurements and shows the worst effective final resolution experimentally obtained for each configuration during the tests performed using different DUT circuits.

TABLE I.   SYSTEM PERFORMANCES

Current Range [A]	±7.85μ	±785n	±78.5n	±7.85n
Full Scale (Y) [S]	±1.57x10⁻⁵	±1.57x10⁻⁶	±1.57x10⁻⁷	±1.57x10⁻⁸
Minimum detectable impedance [Ω]	6.37x10⁴	6.37x10⁵	6.37x10⁶	6.37x10⁷
Min experimental resolution (ENOB) (worst case)	11.3	9	11.4	8.5

In the above table, "Full Scale (Y)" should be considered in terms of admittance using a sinusoidal input amplitude of 1 V_{pp}; its reciprocal is the "Min readable impedance" and "Min experimental resolution (ENOB)" is the minimum effective final resolution experimentally obtained (considering all the experimental tests performed in testing conditions) in terms of effective numbers of bits (ENOB);
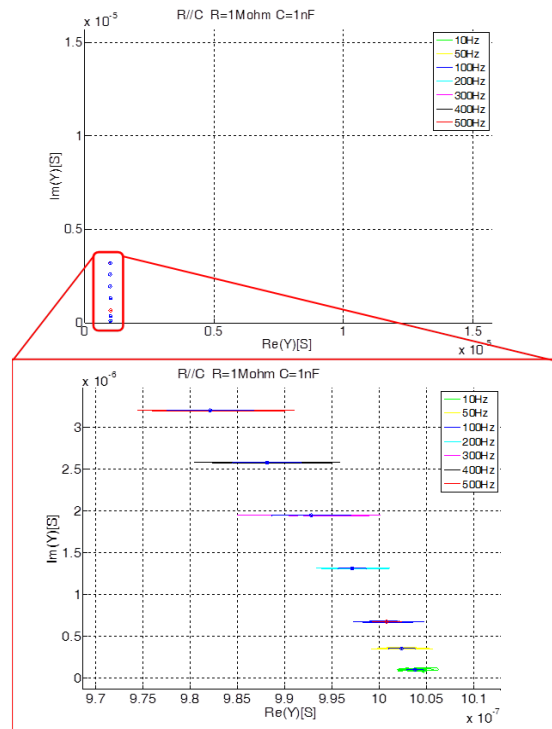
Figure 6.   Example of AC real time admittance measurement of a RC parallel circuit in the Nyqist plane, for different input working frequencies.
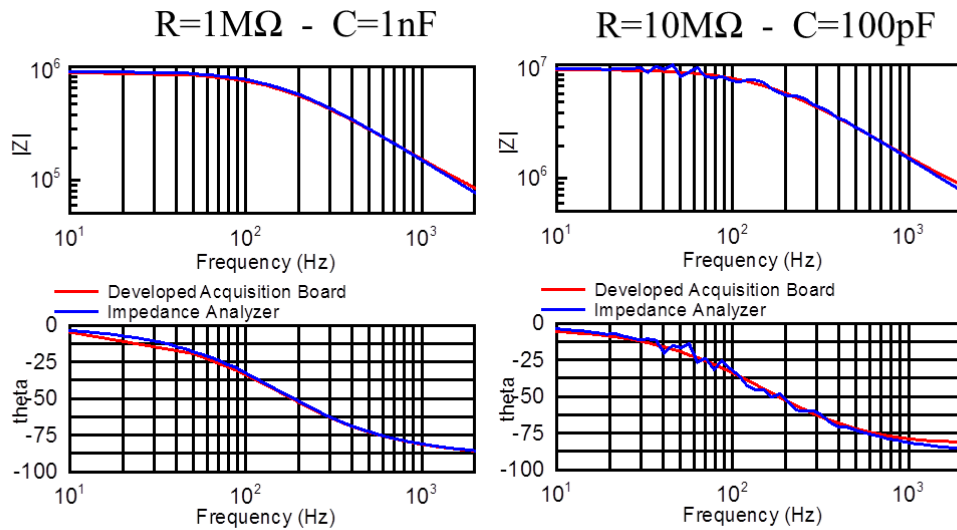
Figure 7.   Bode plots obtained using the developed system interface and the commercial Novocontrol Alpha-A Impedance analyzer with two different parallel RC test circuits.

TABLE II.   COMPARISON WITH IMPEDANCE ANALYZER

	R=1 MΩ - C=1 nF				R=10 MΩ - C=100 pF			
	Acquisition Board		Impedance Analyzer		Acquisition Board		Impedance Analyzer	
	R	C	R	C	R	C	R	C
Fitting error	0.5%	0.5%	0.06%	0.06%	0.6%	0.6%	0.8%	0.8%
Accuracy Error	0.6%	0.5%	0.04%	0.1%	1%	1.1%	0.04%	4.3%

Moreover a comparison between the developed system interface and specific commercial Novocontrol Alpha-A Impedance analyzer, performing 50 points frequency scans in the range 10 Hz-2 KHz on different test circuits were made in order to analyze measurements accuracy in impedance frequency analysis and to calibrate the system. Figure 7 shows the results obtained using two different parallel RC test circuits.

As can be seen the response of the commercial system seems noisier considering the higher impedance DUT; this can be explained considering that in the developed system each frequency point is obtained mediating (by the LabView software interface) the real time AC measurements of a selected number of acquired samples (usually 200 samples), thus reducing the final effective bandwidth of about ten times and thus reducing the external noise.

The obtained points are then saved in a text file in the ZView format and analyzed with ZView software. Table II shows the results in terms of fitting and accuracy errors, where the fitting error is directly calculated by ZView software taking into account the entire spectrum, where accuracy error is calculated using the expression:

$$Accuracy\ Error(\%) = \left| \frac{actual\ value - fitted\ value}{actual\ value} \right| \cdot 100 \qquad (12)$$

The system shows a fair accuracy, which is sufficient for many purposes. The above statement should be taken into account considering the much lower price and smaller sizes of the developed system in comparison with commercial instruments currently used for impedance spectroscopy.

VI.   CONCLUSIONS

A low cost, portable and versatile system, allowing both real time and frequency domain impedance characterization (as well as amperometric measurements) for sensor impedimetric interfaces has been successfully developed and tested. According to the tests, the proposed system has accuracy that is comparable with laboratory instruments on some ranges. Thus, it allows rapid and precise characterization of sensor interfaces at lower cost without highly equipped instrumentation. Moreover, the system could be further shrunk using surface mount device (SMD) implementation allowing to be directly coupled with sensors as readout system. The whole system can be improved and optimized implementing the digital filter stage and input signal generation by means of an FPGA, allowing to further increase the performance in terms of working ranges and time response.

REFERENCES

[1] J. Li, H. T. Ng, and H. Chen, "Carbon nanotubes and nanowires for biological sensing", Methods in molecular biology, vol. 300, 2005, pp. 191-223.

[2] N. S. Ramgir, Y. Yang, and M. Zacharias, "Nanowire-Based Sensors", Small, vol. 6, 2010, pp. 1705-1722.

[3] E. Stern et al., "Label-free biomarker detection from whole blood", Nature Nanotechnology, vol. 5, no. 2, 2010, pp.138-142.

[4] G. Zheng, F. Patolsky, Y. Cui, W. U. Wang, and C. Lieber, "Multiplexed electrical detection of cancer markers with nanowire sensor arrays", Nature Biotechnology, vol. 23, no. 10, 2005, pp. 1294-1301.

[5] S. Sorgenfrei et al., "Label-free single-molecule detection of DNA-hybridization kinetics with a carbon nanotube field-effect transistor", Nature Nanotechnology, vol. 6, no. 2, 2011, pp. 126-132.

[6] M. K. Joo, P. Kang, Y. Kim, G.T. Kim, and S. Kim, "A dual analyzer for real-time impedance and noise spectroscopy of nanoscale devices", Rev. Sci Instrum., vol. 82, no. 3, 2011, 034702.

[7] F. Patolsky, G. Zheng, and C. Lieber, "Fabrication of silicon nanowire devices for ultrasensitive, label-free, real-time detection of biological and chemical", Nature Protocols, vol. 1, no. 4, 2006, pp. 1711–1724.

[8] S. Chen, J. G. Bomer, W.G. van der Wiel, E. T. Carlen, and A. van den Berg, "Top-Down Fabrication of Sub-30 nm Monocrystalline Silicon Nanowires Using Conventional Microfabrication", ACS NANO, vol. 3, no.11, 2009, pp. 3485-3492.

[9] S. Ingebrandt et al., "Label-free detection of single nucleotide polymorphisms utilizing the differential transfer function of field-effect transistors", Biosensors and Bioelectronics, vol. 22, no. 12, 2007, pp. 2834-2840.

[10] Tektronix, Inc., USA Data Sheet. Available at http://www.tek.com/signal-generator/afg3000-function-generator [retrieved: 07, 2012].

[11] National Instruments Corporation, Data Sheet. Available at http://sine.ni.com/nips/cds/view/p/lang/en/nid/201987 [retrieved: 07, 2012].

[12] S. Deng, G. Jian, J. Lei, Z. Hu, and H. Ju, "A glucose biosensor based on direct electrochemistry of glucose oxidase immobilized on nitrogen-doped carbon nanotubes", Biosensors and Bioelectronics, vol. 25, no. 2, 2009, pp. 373-377.

[13] S. Choi, I. Park, Z. Hao, H.Y.N. Holman, and A.P. Pisano, "Quantitative studies of long-term stable, top-down fabricated silicon nanowire pH sensors", Applied Physics A, 2012, doi: 10.1007/s00339-011-6754-9.

[14] M.P. Lu et al., "Semiconducting single-walled carbon nanotubes exposed to distilled water and aqueous solution: Electrical measurement and theoretical calculation", Applied Physics Letters, vol. 88, no. 5, 2006, pp. 053114-053114-3.

[15] O. Knopfmacher et al., "Nernst limit in dual-gated Si-nanowire FET sensors", Nano Letters, vol. 10, no. 6, 2010, pp.2268-2274.

[16] Analog Devices, Inc., Norwood, MA, USA Data Sheet. Available at http://www.analogdevices.com [retrieved: 07, 2012].

[17] Georgi P. Tolstov, Fourier Series, Courier-Dover, 1976.